RSC Advances

ROYAL SOCIETY OF CHEMISTRY

www.rsc.org/advances

A new facile strategy for higher loading of silver nanoparticles onto silica for efficient catalytic reduction of 4-nitrophenol

N. Muthuchamy[1,#], A. Gopalan[2,3,#] and Kwang-Pill Lee[1,2,3,*]

[1]Department of Chemistry Education, Kyungpook National University, Daegu South Korea

[2]Research Institute of Advanced Energy Technology, Kyungpook National University, Daegu South Korea

[3]Department of Nanoscience and Nanotechnology, Kyungpook National University, Daegu Soth Korea

*Corresponding author: kplee@knu.ac.kr ; [#]Authors contributed equally

A new "seed mediated" strategy was designed and demonstrated for the higher loading of silver nanoparticles (Ag NPs) onto silica (SiO_2) to obtain Ag NPs enriched SiO_2 (designated as Ag(E)-SiO_2) catalyst. Simplified two steps were utilized for the preparation of Ag(E)-SiO_2. In the first step, SiO_2 was functionalized with negatively charged p-toluene sulfonic acid ion and embedded with a few Ag NPs (seed) and obtained as Ag(seed)-SiO_2(p-TSA^-). In the subsequent step, excessive Ag^+ ions were pre-concentrated onto SiO_2 surface using the negative charges on the SiO_2 surface and reduced to Ag NPs. The pre-existing Ag NPs(seed) and pre-concetrated Ag^+ ions enabled the growth of further layer of Ag NPs to obtain Ag(E)-SiO_2. Results from FTIR spectroscopy, X-ray diffraction (XRD) and X-ray photoelectron spectroscopy (XPS) measurements clearly supported our strategy of simultaneous functionalization of SiO_2 and Ag(seed) formation through the first step. Detailed FESEM, TEM and XPS analysis revealed higher loading (~80 weight % (wt%)) of Ag NPs in Ag(E)-SiO_2 with a metallic valence state. The catalysts, Ag(seed)-SiO2(p-TSA^-) and Ag(E)-SiO_2, containing low Ag (~10 wt%) and higher Ag loading (~80 wt%) of Ag NPs, respectively, were tested for the reduction of toxic organic compounds such as 4-nitrophenol (4-NP) and methylene blue (MB). The Ag(E)-SiO_2 catalyst exhibited superior catalytic performances for 4-NP/MB reduction as compared to Ag(seed)-SiO_2(p-TSA^-) (conventional) as well over several other Ag NPs supported catalysts reported in the literature. The enhanced catalytic performance for Ag(E)-SiO_2 for 4-NP and MB reduction suggested

that our new strategy is promising for the preparation of efficient supported catalyst for water purification and related applications.

1. Introduction

A great deal of research has been carried in the area of catalytic applications of silver nanoparticles (Ag NPs) on a variety of organic reactions.[1-4] Nevertheless, the catalytic efficiency and stability of Ag NPs are often hampered by aggregation or congrogation of particles due to interparticle interactions through var der Waals forces and high surface energies. To solve these problems, techniques have been developed to immobilize Ag NPs onto a desired substrate (support) and generate Ag NP coated support composite structures.[5-7] The catalytic properties of supported-Ag metal catalysts are found to be mainly dependent on various factors that include size distribution and amount of Ag NPs particles as well the interactions between Ag NPs and the support.[8-10] Specifically, the catalytic performances of the Ag-SiO_2 supported catalysts are restricted by two main problems; the low surface coverage of Ag NPs onto SiO_2 (support) and ineffective binding between the support and Ag NPs.[11,12] An optimal Ag-SiO_2 catalyst should balance these requirements to have high efficiencies for catalytic reactions. For achiving high afficiency for Ag supported catalyst, it has been reported that both the support and immobilized Ag NPs play critical roles.[13] The stability of the support catalyst can be enchanched by incorporating functional groups such as $–NH_2$ etc. in the support.[14] However, the methods to increase the amount of Ag NP onto the surface of support are scarce.

Out of the various supports, silica (SiO_2) delivers several advantages that include simplicity of preparation through known synthetic methods, high surface activity, narrow size distribution and large availability from commercial source.[15] Untill now, several approaches or methods have been developed to coat SiO_2 with Ag particles.[11-13,16] However, the direct loading of Ag NPs onto SiO_2 particles was reported to the difficult due to the ineffective interactions between SiO_2 surface and metal particles. Thus, the prior surface functionalization or modification of the

support (SiO_2) matrix is still an inevitable step for developing efficient Ag-SiO_2 catalyst. By tuning the surface functionality of the support SiO_2 matrix, it would not only possible to load maximum catalyst (Ag NP) particles, but also generate synergistic interactions between Ag NPs and support material, which is turn enhance catalytic activity and stability. Hence, there is a need to functionalize or modify the SiO_2 with special functional groups as well to develop new strategies to increase the Ag content onto SiO_2 support. On the basis of genuine requirements for the synthesis of efficient Ag-SiO_2 catalyst as mentioned above, in this paper, we propose an innovative and simple procedure for preparing Ag enriched silica (Ag(E)-SiO_2) catalyst with higher loading of Ag NPs utilizing a 'new seed mediated' strategy. Based on our results, we demonstrated that Ag(E)-SiO_2 exhibited excellent catalytic activities as compared to earlier reports on Ag-SiO_2 catalysts prepared through conventional approaches.

"*Seeding*" strategies are generally used to generate larger amount/sized metal nanoparticles (MNPs), taking into the advantage of the surface catalysis. "The seeding" methodology is a typical heterogeneous process and generally done to by-pass the spontaneous nucleation or to uncouple nucleation from the crystal growth.[17] In a typical "seed mediated" growth of MNPs, the pre-formed seed MNPs are added into a growth solution of metal salt. Due to the fact that activation energy for metal reduction is significantly lower in heterogeneous condition than that for homogeneous nucleation, auto-catalytic growth of metal particles on the pre-existing seed is preferentially occurs. The "seed mediated" growth effectively separates the nucleation and growth of NPs formation and enhances the particle dispersity, relative to the general synthetic methods.[18] Typically, anchoring of MNPs to on SiO_2 support is carried out through two routes; (i) insitu electroless platting of MNPs onto surface modified support and (ii) anchoring the pre-formed MNPs on to SiO_2 support.[19,20] The "seed mediated" growth strategy can also be utilized

to enrich MNPs onto support materials.[21] However, reports reveal that preparation of SiO_2-MNP composite microsphere through "seed mediated" growth requires complex stages such as separate preparation of SiO_2 and MNPs, surface modification of SiO_2 or MNPs and subsequent loading of MNPs on the support matrix. A simple strategy for the high loading of MNPs onto SiO_2 support, which can minimize the multiple stages, such as preparation of seed-MNP/support, functionalization of support or MNPs, loading of metal ions onto the support and enhancing the interaction between MNP and support, is highly warranted.

In this work, a proof of concept has been demonstrated through reporting the preparation of excessive Ag NP loaded SiO_2 (Ag(E)-SiO_2) supported catalyst through our new simple synthetic strategy. The proposed design for the synthesis of Ag(E)-SiO_2 involves simple two steps (Scheme-1); (i) preparation of Ag NP (seed) incorporated p-toluene sulfonic acid anion (p-TSA^-) functionalized SiO_2 spheres (designated as Ag(seed)-SiO_2(p-TSA^-)) and excessive loading of Ag NPs onto Ag(seed)-SiO_2(p-TSA^-). The highlight of the present design for the preparation Ag(E)-SiO_2 catalyst was the simultaneous formation of functionalized support matrix and incorporation of Ag NPs(seed) through a single synthetic step which facilitates the subsequent accumulation of Ag^+ ions and higher loading of Ag NPs (Scheme-1 (step i)). The synthesized Ag(E)-SiO_2, having higher loading (~80 wt%) of Ag, was utilized as the catalyst toward reduction toxic organic compounds such as 4-nitrophenol (4-NP) and the dye, e.g. methylene blue (MB) and the catalytic efficiencies were compared with Ag-SiO_2 catalysts prepared by conventional metal catalysts. The Ag(E)-SiO_2 catalyst clearly exhibited enhanced reactivity for the reduction of 4-NP and MB over the conventional Ag-SiO_2 catalysts reported in literature (Table 1 and 2) and provided the scope for the use of Ag(E)-SiO_2 in water purification and other catalytic reductions.

2. Experimental section

2.1 Materials

The chemicals, TMSPA, p-TSA, 4-NP, triethylamine and $NaBH_4$ were obtained from Sigma-Aldrich (Korea). MB (Duksan, Korea), sodium citrate (SC) ammonium persulphate (APS) (DC chemical, Korea) and silver nitrate (Kojime chemicals, Korea) were used as received.

2.2 Synthesis of Ag(E)-SiO_2

Synthesis of Ag(E)-SiO_2 involves two major steps (Scheme-1); i) preparation of "seed" Ag NPs embedded ($p\text{-}TSA^-$) functionalized SiO_2 sphere (Ag(seed)-SiO_2($p\text{-}TSA^-$)) and ii) excessive loading of Ag NPs onto Ag(seed)-SiO_2($p\text{-}TSA^-$).

2.2.1 Preparation of Ag(seed)-SiO_2($p\text{-}TSA^-$)

In a typical reaction, the solution A (50 mL of 75 mM TMSPA in p-TSA) and solution B (60 mL of 200 mM of Ag NO_3 in 0.1M p-TSA) were prepared and cooled to 5 ^{0}C. The solution B was added dropwise to solution A (kept at 5 ^{0}C) with vigorous stirring. The mixture was kept in stirring condition for 6 hours. The Ag(seed)-SiO_2($p\text{-}TSA^-$) was obtained by centrifugation of the mixture. The residue was washed repeatedly with p-TSA till the filtrate was colorless and dried at 80 ^{0}C for 12 h.

2.2.2 Higher loading of Ag NPs onto Ag(seed)-SiO_2($p\text{-}TSA^-$)

About 9.5 mL of an aqueous solution containing 0.2 M of SC was prepared and dispersed with 100 mg of Ag(seed)-SiO_2($p\text{-}TSA^-$) by continuous stirring. The solution temperature was raised until it reached 80 ^{0}C. About 500 μL of 0.5M Ag NO_3 was injected into the above hot mixture

solution and kept stirred for 5 min. The reaction mixture was there after cooled to room temperature. The mixture was filtered, washed with water and dried at 80 ^{0}C for 12 h. Pilot expriments, were first performed on the preparation of Pristine SiO_2 (without embedding Ag NPs) was prepared by adopting the similar procedure as described in 2.2.1, but by using APS instead of Ag NPs and the conditions were optimized to obtain uniform sized SiO_2 particles.

2.3 Catalytic reduction of 4-Nitrophenol

The catalytic properties of the Ag(E)-SiO_2 and Ag(seed)-SiO_2(p-TSA^-) were investigated via the reduction of 4-NP in the presence of excess concentration of $NaBH_4$ (> 100 times)[22] and UV–visible spectroscopy was used to follow the kinetics of catalytic reduction of 4-NP under different experimental conditions (SI: Table. T1). In a typical kinetic experiment, 18 mL of a freshly prepared aqueous solution containing 0.5 mM of 4-NP and 0.25 g/L catalyst was taken in a quartz cuvette stirred vigorously for 30 min. About 2 mL of 50 mM fresh $NaBH_4$ aqueous solution was added to the mixture suddenly (time lapse of 30 s) and the temperature was maintained at 278 ^{0}K. The solution was carefully mixed by shaking gently. The suspension was sampled at certain time intervals, filtered and UV-visible spectra were recorded after proper dilution to obtain successive information. The catalytic conversion efficiency of 4-NP (CE_{NP} (%)) was calculated by the absorbance decrease of the electronic bond at 400 nm using

$$\boldsymbol{CE_{NP}}(\%) = \frac{\boldsymbol{A_0 - A_t}}{\boldsymbol{A_0}} \times \mathbf{100}$$

Where $\boldsymbol{A_t}$ is the absorbance of 4-NP (λ=400 nm) at any time t and $\boldsymbol{A_0}$ is the initial absorbance of 4-NP measured at zero time. The effects of 4-NP concentration, quantity of catalyst, pH, reaction time and temperature on the rate of the reaction were followed.

The catalytic recycling capability was determined by filtration of the catalyst after the reaction had completed (CE=100%), washed thoroughly with water and ethanol, followed by drying at 30 ^{o}C in a vacuum oven. The catalyst was again redistributed in a fresh reaction system and the catalytic experiments were performed using the same reaction conditions as before. This has been done to ensure whether the catalyst was recoverable without loss of mass and the recycled catalyst could be subsequently used without much decrease in CE_{NP}%. The recycling experiments was repeated five times.

2.4 Catalytic reduction of MB

The catalytic activities of the as prepared Ag(E)-SiO_2 and Ag(seed)-SiO_2(p-TSA^-) were investigated for the reduction of MB in the presence of the $NaBH_4$. In a typical experiment, an 18 mL solution of MB ($5x10^{-4}$M) was dispersed with 0.25 g/L of the catalyst. About 2 mL of 50 mM $NaBH_4$ was added quickly under constant stirring (time lapse of 30 s) and the temperature was kept at 278 ^{0}K. The reduction reaction was followed by monitoring the MB concentration throughout the reaction by UV-visible spectroscopy. Importantly, no visible color change was observed in the absence of catalysts.

2.5 Instruments

The size and morphology of the synthesized materials were determined by field-emission scanning electron microscopy (FE-SEM) equipped with an energy dispersive X-ray spectrometer (EDX) (FE-SEM, S-4300 & EDX-350, Hitachi, Japan). Transmission electron microscopy observations were performed on a HD-2300, Hitachi, TEM (Japan) operating at 200 kV. The crystallographic structure of the products was investigated by X-ray diffraction (XRD, Quantera SXM, ULVAC-PHI, Japan) using Cu-K radiation (l = 1.5406 ˚A) in the 2θ range 20 to 85^{0}. X-ray photoelectron spectroscopy (XPS) measurements were conducted by using a Quantera SXM,

ULVAC-PHI with monochromatic Al-Kα radiation in the binding energy range 0-1400 eV. Fourier transform infrared (FTIR) spectra were recorded (1486.6 eV) on a Bomem MB 100 FT-IR spectrometer (ABB Bomem, QC, Canada) in the wavenumber range 400-4000 cm^{-1}. UV-vis spectra were recorded using a Cary 5000, Agilent (Korea) UV/vis/NIR spectrometer.

3. Results and discussion

3.1 Synthesis of Ag(E)-SiO_2

Several synthesis strategies/methods have been developed by earlier workers[5-7,11-13,16] to impregnate Ag NPs onto SiO_2, but those were restricted with a minimum loading of Ag NPs (<10%) and/or involve multiple steps. To mention specifically, two of the synthetic approaches are particularly interesting for the formation of Ag shell onto SiO_2 support. In the first approach, namely electroless platting, compound such as $SnCl_2$ is first used to activate the core SiO_2 surface.[23] To obtain denser coating of Ag NPs shell onto SiO_2 support, two repeated steps, such as adsorption of Sn^{2+} ions onto SiO_2 surface and subsequently the adsorption of Ag^+ ions, were utilized. In the second approach, electrostatic association of alternatively charged species was utilized by a layer by layer technique to cover the Ag particles onto SiO_2 surface.[24,25] However, in both of the approaches, dense coverage of Ag particles could not be achieved by a simple step. And, the two methods for creating dense coverage of Ag particles on SiO_2 are time consuming and tedious. Therefore, the development of simple strategy to prepare SiO_2 sphere covered with a uniform and dense metallic Ag nano-shell still remains a great challenge to material scientists.

Motivated by the state of art, in the present study we introduced the new strategy for higher loading of Ag NPs onto (>80 wt %) SiO_2 support which involved the combination of two simple steps. In the first step, simultaneous formation of functionalized SiO_2 particles and Ag NPs (seed) (low loading) was achieved to obtain Ag(seed)-SiO_2(p-TSA^-) by the addition of

$AgNO_3$ to a solution of TMSPA in p-TSA (Scheme 1, step (i)). In our approach, TMSPA and amphiphilic p-TSA were specifically chosen as silica precursor and medium, respectively, to obtain spherical SiO_2 particles containing p-TSA^- groups at the SiO_2 surface. The molecules of p-TSA self-assembled into spherical micelles in aqueous solution and augmented the formation of spherical SiO_2 particles.[26-28] The preparation of Ag(seed)-SiO_2(p-TSA^-) provides scope for improving or enhancing the Ag NPs loading by subsequent step and therefore differ from the conventional method of Ag-SiO_2 catalyst preparation with a lower loading of Ag metal. [5-7,11-13] The absence of adequate functionalization at the SiO_2 support in the conventional Ag-SiO_2 catalyst preparation restricts the excessive loading of Ag NPs by the subsequent step. A plausible mechanism formation for the Ag(E)-SiO_2 is illustrated in Scheme 1. Typically, the formation of p-TSA^- functionalized SiO_2 (SiO_2(p-TSA^-)) involves hydrolysis of -OMe groups, polycondensation of silanol groups and oxidation of $-NH_2$ groups in TMSPA to result SiO_2 network comprising of polyaniline (PANI) chains.[29,30] Under the experimental conditions, the amine/imine units in the PANI chains within SiO_2 support existed in doped state (Evidences are provided in section 3.2.) with p-TSA^- as the counter balancing anions for the positive charges on nitrogen atoms. As a result, the surface of SiO_2 contained p-TSA^- ions. Also, Ag NPs were formed by the concurrent reduction of Ag^+ ions and embedded into SiO_2(p-TSA^-), to result Ag NPs (seed)-SiO_2(p-TSA^-). Interestingly, in the step (ii) (Scheme 1), the negatively charged p-TSA^- ions on the surface of Ag(seed)-SiO_2(p-TSA^-) were utilized to bind Ag^+ ions through electrostatic interactions with p-TSA^- to pre-concentrate the Ag^+ ions on the SiO_2 surface. Besides, Ag^+ ions were co-ordinated through the un-protonated amine/imine units of PANI chains. As a result, excessive Ag^+ ions were pre-concentrated on the surface of SiO_2 for further reduction to Ag NPs. The excessive loading of Ag NPs onto SiO_2 was subsequently achieved by

reduction of Ag^+ ions by SC (Scheme 1, step (ii)). Thus, Ag(E)-SiO_2 particles with higher loading of Ag NPs were obtained through our new strategy.

In brief, the first stage of our proposed strategy of the synthesis of Ag(E)-SiO_2 involved the production of SiO_2 particles with a minimum number of distributed Ag NPs as the seed. It is that the sizes and uniformity of SiO_2 particles as well as the Ag NPs have great influence on catalytic properties.[31] As for the synthesis of SiO_2 particles with uniform particle size distributions, three main synthetic methods were earlier proposed, namely, microemulsions, hydrolysis of elemental Silicon and Stober's process.[32-35] While the emulsion method requires larger amount of surfactant and associated tedious post purification procedures, the silicon hydrolysis method needs prior activation of silica core with toxic hydrofluoric acid and alcohol. Stober's process is the simplest and effective because the reactants are normal and reaction conditions are tunable to control the particle size distributions and shape by modification of synthetic factors, such as temperature, pH and concentration of reactants. Since Stober prepared SiO_2 particles in the range 0.05 to 2 μM through the hydrolysis and condensation of alkyl silicates (such as tetraethoxy orthosilicate) in alcoholic solutions, many researchers prepared SiO_2 particles in different sizes by adjusting the experimental conditions.[36,37] However, Stober's procedures utilized alcohol, which was deterrent for catalytic applications. In this work, we employed a modified Stober's synthesis, which did not involve alcohol as the reactant and used TMSPA, the trimethoxy substituted silica precursor with a propyl aniline group, for the simultaneous formation and functionalization of the SiO_2 particles. The SiO_2 forming reaction was initiated with Ag^+ ions, and the Ag^+ ions in the process of reaction were reduced to Ag^0 particles. Importantly, we utilized an optimized experimental conditions with a molar ratio of TMSPA:$AgNO_3$:p-TSA as 3:12:10, to obtain uniform size distributions of both SiO_2 particles

and Ag NPs (Fig. 1). The sizes of the Ag NPs produced at the seed stage subsequently controlled the sizes of Ag NPs at the excessive loading stage.

3.2 Characterization of Ag(E)-SiO_2

Fig.1 compares the SEM images of SiO_2 particles without loading the seed Ag NPs (pristine SiO_2, PTMSPA) and SiO_2 particles after loaded with seed Ag NPs (Ag(seed)-SiO_2(p-TSA^-)). Fig.1A shows the FESEM image of pristine SiO_2 (without loading of Ag NPs), which informs that large number of particles (>89%) were spherical with uniform sizes (~600 nm) having smooth external surfaces. Besides, a lesser proportion (~11%) of smaller sized spherical particles with random sizes were also seen in the FESEM image of pristine SiO_2. The molar ratio of TMSPA:$AgNO_3$:p-TSA was optimized as 3:12:10 after performing reactions with different other molar ratios of TMSPA:$AgNO_3$:p-TSA (see: section 2.2.2). Experiments with the other molar ratios of TMSPA:$AgNO_3$:p-TSA than 3:12:10, neither produced spherical particles noruniform sizes. For the synthesis of Ag(seed)-SiO_2(p-TSA^-), we utilized the concentrations of p-TSA and TMSPA as similar to the synthesis pristine SiO_2, but $AgNO_3$ was used instead of APS. Therefore, the experimental conditions for the preparation of Ag(seed)-SiO_2(p-TSA^-) was maintained with molar ratio of TMSPA:$AgNO_3$:p-TSA as 3:12:10. The surface morphology of Ag(seed)-SiO_2(p-TSA^-) (Fig. 1B) shows spherical SiO_2 particles with similar sizes (~600 nm) as observed with pristine SiO_2 (Fig. 1A). However, the surfaces of SiO_2 particles were rough with smaller sized particles distributed on the surfaces as bumps. The TEM image of Ag(seed)-SiO_2(p-TSA^-) (Fig. 2A) (Fig. 1B) contained smaller number of nearly uniform sized spherical Ag NPs. Also, TEM image of Ag NPs in Fig. 2A clearly revealed that Ag NPs were tethered onto the surface of SiO_2 particles. The sizes of seed Ag NPs in the as prepared Ag(seed)-SiO_2(p-TSA^-) were nearly uniform with a narrow sizes in the range from 5.8 nm to 7 nm (Fig. 2A). Likewise, the TEM

image of Ag(E)-SiO_2 (Fig. 2B) were utilized to infer the sizes of Ag particles in the Ag(E)-SiO_2. By analyzing the sizes of nearly one hundred Ag NPs on the shell of SiO_2 microspheres (Fig. 2B), it is inferred that majority of Ag NPs (>86%) are having sizes in the range from 6.0 to 6.8 nm. Few larger sized particles (~8 to 10 nm) were also found that could arise from the nucleation overgrowth Ag on the seed Ag NP.

The EDAX spectra recorded for Ag(E)-SiO_2 and Ag(seed)-SiO_2(p-TSA^-) (See: supporting information (SI), SI: Fig. S1) provide clear difference in the Ag elemental composition at the "Seed" and "extended growth" stages. Typically, EDAX spectrum of Ag(seed)-SiO_2(p-TSA^-) (SI: Fig. S1A) informed that about 9.9 weight % of Ag was distributed within Ag(seed)-SiO_2(p-TSA^-). Turning to TEM image of Ag(E)-SiO_2 (Fig. 2B), large number of Ag NPs could be noticed onto the entire surface of SiO_2 particles (Fig. 2B). The EDAX spectrum of Ag(E)-SiO_2 (SI: Fig. S1B) revealed that nearly ~80 weight % of Ag was present in it. The Ag loading in Ag(E)-SiO_2 is therefore much higher as compared to the Ag ~9.9% weight % in the case of Ag(seed)-SiO_2(p-TSA^-) (SI: Fig. S1A), validating the importance of "seed mediated growth" approach (Scheme.1). Importantly, EDAX elemental analysis of Ag(seed)-SiO_2(p-TSA^-) (SI: Fig. S1A) and Ag(E)-SiO_2 (SI: Fig. S1B) informed the presence of nearly 2 % (atomic weight) of sulfur (S) element. The 'S' in these SiO_2 materials was originated from p-TSA. It has been demonstrated by previous researchers that activities of supported metal catalysts depend on metal particle sizes, the size/nature of the support and amount of catalyst particles on the support.[38-40] The sizes of Ag NPs anchored on SiO_2 or other supports reported by other researchers are presented SI. Table. T2. Our proposed strategy for the preparation of Ag(E)-SiO_2 not only provided denser Ag coating (~86 wt%) but also produced Ag NPs with smaller sizes (6

nm to 8 nm) and narrow distributions. Hence, we anticipated that Ag(E)-SiO_2 could be an efficient catalyst as compared to many of the other Ag-SiO_2 catalysts reported in literature.

The phase composition and crystal structure of the components in Ag(E)-SiO_2, Ag(seed)-SiO_2(p-TSA^-) and pristine SiO_2 were investigated from the respective XRD patterns (Fig. 3). While XRD patterns of Ag(E)-SiO_2 (Fig. 3, curve a) and Ag(seed)-SiO_2(p-TSA^-) (Fig. 3, curve b) showed a number of crystalline diffraction peaks at 2θ range 30^o to 80^o, the XRD pattern of pristine SiO_2 (Fig. 3, curve c) revealed only a broad amorphous peak around 2θ = 21°. The broad band in the 2θ range 20–30° for pristine SiO_2 corresponds to the periodicity parallel to the PANI chains.[41,42] The absence of crystalline peaks in the XRD pattern of pristine SiO_2 (Fig. 3, curve c) suggests the predominant amorphous characteristics of pristine SiO_2. The XRD pattern of Ag(seed)-SiO_2(p-TSA^-) (curve b) and Ag(E)-SiO_2 (curve a) exhibit reflection peaks at 2θ = 32.2^o, 38.2^o, 44.6^o, 64.4^o and 77.4°, that correspond to (112), (111), (200), (220) and (311) face centered cubic (fcc) crystalline structure of Ag particles. On the contrary, as compared to the XRD pattern of pristine SiO_2 (curve c), the XRD patterns of Ag(seed)-SiO_2(p-TSA^-) (curve b) and Ag(E)-SiO_2 (curve a) showed strong reflection patterns of silicon at 2θ values , 27.8^o (111), 46.3^o (220) , 57.5^o (311), 67.4^o (400) and (331) that correspond to crystalline planes of silicon. Thus, XRD results demonstrate that SiO_2 generated upon treatment of TMPSPA of with $AgNO_3$ was crystalline.[43] XRD pattern of Ag(E)-SiO_2 exhibited sharp and intense crystalline peaks of Ag particles (Fig. 3, curve a) as compared to Ag crystalline peaks in the XRD pattern of Ag(seed)-SiO_2(p-TSA^-) (curve b). Using the Debye-Scherrer equation, the average crystalline size of Ag particles in Ag(E)-SiO_2 was determined to be 7 nm, which is in close agreement with the size noticed through the TEM image (Fig. 2 A).

The elemental composition, oxidation state of Ag and the doping state of PANI chains in Ag(seed)-SiO_2(p-TSA^-) and Ag(E)-SiO_2 were investigated by XPS analysis. The survey level XPS spectrum showed sharp peaks of C1s (284 eV), O1s (532 eV), N1s (398 eV), Si2p (101 eV) for pristine SiO_2 (Fig. 4 A(c)) and an additional peak (~367 eV) of Ag3d for Ag(seed)-SiO_2(p-TSA^-) (Fig. 4 A(b)) and Ag (E)-SiO_2 (Fig. 4 A(a)). The fine scanned Ag3d XPS spectrum of Ag(E)-SiO_2 (Fig. 4B, (a)) showed double binding energy (BE) peaks at 367.01 eV and 367.14 eV for $Ag3d_{5/2}$ and $Ag3d_{3/2}$, respective. Similarly, BE peaks were observed at 373.01 eV and 373.21 eV, respectively, for Ag(seed)-SiO_2(p-TSA^-) (Fig. 4B, (b)). The spin-orbit splitting of 3d doublet was observed to be ~6.0 eV in both the cases. The XPS analyses of Ag3d spectrum informed that Ag on SiO_2 support predominantly exists as metallic Ag^0.[44] However, the shifts in BEs of $Ag3d_{5/2}$ and $Ag3d_{3/2}$ state for between Ag(E)-SiO_2 and Ag(seed)-SiO_2(p-TSA^-) are attributed to the size effects of the crystalline Ag NPs in these meterials.[45,46] The N1s core level spectra of the materials provide information about the different nitrogen states (-N=, -N^+- and -NH-) in PANI chains. The peaks around ~398 eV, 400 and 405 eV are ascribed to quinoid imine (-N=), the benzenoid imine (-NH-) and positively charged nitrogen (-N^+-), respectively.[47] The peak area ratio of (-N=) to (-NH-) for the Ag(E)-SiO_2 was 0.57, which suggested the existence of significant proportion of imine (-N=) and protonated nitrogen (C-N^+-) indicating that Ag(seed)-SiO_2(p-TSA^-) was in doped state. The positive charges on the nitrogen atoms could be counter balanced by the p-TSA^- anions. Thus, XPS results validate that Ag(seed) included SiO_2 contains surface p-TSA^- which could bind Ag^+ ions for further loading of Ag NPs.

FTIR spectra (SI: Fig. S2) of Ag(E)-SiO_2, Ag(seed)-SiO_2(p-TSA^-) and pristine SiO_2 show the characteristic vibrational bands of silica frame work (Si-O-Si) (~1090 cm^{-1}) and PANI chains (around 1590 and 1500 cm^{-1}).[26] Typically, the intense absorption bands around 1090 cm^{-1},

800-810 cm^{-1} and 460-470 cm^{-1} are assigned to asymmetric and symmetric stretching vibration of the Si-O-Si frame work of SiO_2. The broad absorption bands around 3420-3450 cm^{-1} and 960-970 cm^{-1} correspond to the Si-OH stretching and bending vibrations, respectively. The absorption intensities of Si-O-Si vibrational bands were significantly decreased for Ag(seed)-SiO_2(p-TSA^-) and Ag(E)-SiO_2 as compared to the vibrational bands of pristine SiO_2. The vibrational bands observed around 1590 and 1500 cm^{-1} are attributed to quinoid N=Q=N ring stretching (Q=quinoid unit) and benzenoid (N-B-N) (B= benzenoid unit) stretching modes of PANI chains. The peak at 1240 cm^{-1} is assigned to the $C–N^+$ stretching vibration of PANI chains and its existence informs that the amine/imine units of PANI chains in these materials are in the doped states.[48, 49] The peaks for asymmetric and symmetric O=S=O stretching vibrations of SO_3^- groups overlap with Si-O-Si stretching vibrational band.[50]

3.3 Catalytic performance of Ag(E)-SiO_2 catalyst

Nitroaromatic compounds (especially 4-NP) and few dyes (such as MB) are identified as toxic pollutants found generally in industrial wastes and industrial effluents, as they are discharged into groundwater from textile, paper, plastic, dye and pharmaceutical industries.[51,52] The toxic 4-NP can be reduced to non-toxic 4-aminophenol (4-AP), an useful material for several pharmaceutical applications. Catalytic reduction of 4-NP and dyes with an excess amount of $NaBH_4$ have been used as model reactions to evaluate the catalytic performance of metal nanoparticles either alone or loaded onto supports.[53]

3.3.1 Degradation of 4-NP

The catalytic performances of the as-prepared Ag(E)-SiO_2 catalyst were evaluated for the reduction of 4-NP under different experimental conditions (SI: Table.T1). In all of the 4-NP reduction experiments, a far excessive concentration of $NaBH_4$ (50 mM) was used as compared

to the concentrations of 4-NP (0.5 mM), to keep the reduction rates independent of the concentration of $NaBH_4$. The progress of reduction reaction was monitored by following the absorbance changes using UV-visible spectroscopy as well as through visual disappearance of yellow colour of the 4-NP. An aqueous solution of 4-NP was pale yellow in colour (naked eye) and exhibited a peak at 317 nm (UV-visible spectroscopy). After adding $NaBH_4$ into the aqueous solution of 4-NP, the colour of the solution changed from light yellow to greenish yellow (naked eye) due to the formation of 4-nitrophenolate ion. The formation of phenolate ions was evident by the appearance of a peak at 400 nm (UV-visible spectroscopy). In the absence of catalyst, the colour of phenolate ion (greenish yellow) was stable for several hours (up to 4 h). However, the colour of the 4-nitrophenolate changed with time after the addition of Ag(seed)-SiO_2(p-TSA^-) or Ag(E)-SiO_2 catalyst. The characteristic peak at 400 nm, that is ascribed to 4-nitrophenolate ion, gradually decreased with time and signified the reduction of 4-NP.[54,55] A new peak that corresponds to the formation of 4-AP appeared at 300 nm during the reduction of 4-NP. It is also to be noted that the presence of pristine SiO_2 did not change the absorbance value at 400 nm significantly over a long period (>4h), which informed the negligible transformation of 4-NP to 4-AP with pristine SiO_2 catalyst (SI: Fig. S3).

The catalytic performances of Ag(E)-SiO_2 and Ag(seed)-SiO_2(p-TSA^-) were compared towards reduction of 4-NP. Fig. 5 provides the time dependent UV-visible absorption spectra recorded during the course of 4-NP reduction in the presence of Ag(E)-SiO_2 (Fig. 5A) or Ag(seed)-SiO_2(p-TSA^-) (Fig. 5B) catalyst. When the reduction of 4-NP was catalysed by Ag(E)-SiO_2, nearly f100% CE was achieved by 10 min for a concentration of 4-NP as $5x10^{-4}$ M with a catalyst loading of 0.25g/L (Fig.5A). However, for a similar experimental condition, Ag(seed)-SiO_2(p-TSA^-) catalyst exhibited only a CE of 64% even after longer period (>25 min) . The CE

values of the two catalysts, Ag(E)-SiO_2 and Ag(seed)-SiO_2(p-TSA^-) (Fig. 6A-B) were also compared for a higher initial 4-NP concentration ($1x10^{-3}$M). Nearly, 100% CE was witnessed by 18 min for Ag(E)-SiO_2 catalyst (Fig.6 A). However, Ag(seed)-SiO_2(p-TSA^-) catalyst showed only a CE of 25% by 18 min. Thus, we conformed that Ag(E)-SiO_2 catalyst showed superior performances over the conventionally prepared Ag(seed)-SiO_2(p-TSA^-) catalyst.

More quantitative data analysis was done through correlating the changes in absorbances at 400 nm over time for different experimental conditions (SI: Table. T1). On general considerations, the rate of the reduction of 4-NP (ϑ_{NP}) is expected to depend on the experimental conditions according to:

$$\boldsymbol{\vartheta_{NP} = \frac{-d[4-NP]}{dt} = k\,[4-NP]^x[Ag(E)-SiO_2]^y[NaBH_4]^z} \quad (1)$$

where [4-NP] and [$NaBH_4$] are the concentration of 4-NP and $NaBH_4$, respectively. The constant k represents the rate constant for the reduction of 4-NP. The concentration exponent x, y, and z, in equation (1) represents the kinetic order with respect to 4-NP, Ag(E)-SiO_2 catalyst and $NaBH_4$, respectively. Since the concentration of $NaBH_4$ was maintained far excessive than that of 4-NP, the $\vartheta_{NP}$is presumed to be independent of [$NaBH_4$], which allows the reduction of 4-NP to be evaluated by the pseudo-first order kinetics.

$$\boldsymbol{\vartheta_{NP} = \frac{-d[4-NP]}{dt} = k_{app}\,[4-NP]^x[Ag(E)-SiO_2]^y} \quad (2)$$

Here, k_{app} is the apparent (pseudo-first order) rate constant for the reduction of 4-NP.

Detailed batch experiments were performed to follow the kinetics and to understand the influence of experimental conditions such as [4-NP] and amount of catalyst on ϑ_{NP} (SI: Table.T1). While performing these experiments, the concentration of $NaBH_4$ (50 mM) or the amount of catalyst (0.25 g/L) or [4-NP] was kept constant (SI: Table.T1). The plots $\ln(c_o/c_t)$ *versus* time (Fig. 7(A-B)) for Ag(E)-SiO_2 and Ag(seed)-SiO_2(p-TSA^-) catalysed 4-NP reduction

reactions were drawn for two typical experimental conditions. Linear relations of the plots of $\ln(c_t/c_0)$ *versus* time were observed for the catalytic reduction of 4-NP with Ag(E)-SiO_2 and Ag(seed)-SiO_2(p-TSA^-), indicating that the reaction followed pseudo-first order kinetics. The k_{app} values were estimated from the slopes of the straight lines (Fig. 7A and Fig. 7B). Likewise, the value of k_{app} were deduced for the reduction of 4-NP using Ag(E)-SiO_2 and Ag(seed)-SiO_2(p-TSA^-) catalyst for various experimental conditions (SI: Table.T1) and the average value of k_{app} was estimated as 10.56×10^{-3} s^{-1} for Ag(E)-SiO_2 and as 2.48×10^{-3} s^{-1} for Ag(seed)-SiO_2(p-TSA^-). The k_{app} for Ag(E)-SiO_2 was significantly (4 times) higher than with Ag(seed)-SiO_2(p-TSA^-) catalyst. Table. 1 gives an overall comparison catalytic rate constant of the present catalyst with other Ag based catalysts such as pristine Ag NPs,[56] Ag alloys,[57] Ag NP supported polymers,[58-61] Ag-carbon,[62] Ag-SiO_2[63,65,66] and many other support Ag catalysts[56,63,64] operated under different experimental parameters. The superiority of the Ag(E)-SiO_2 catalyst for 4-NP reduction is clearly evident from the catalytic efficiency comparison as presented in Table. 1. The enhanced catalytic activity of Ag(E)-SiO_2 is attributed to the higher loading Ag NPs and good distribution of small sized Ag NPs (~7 nm) on the SiO_2 surface as inferred from HR-TEM (Fig. 2B) image. The k_{app} value of Ag (E)-SiO_2 for the reduction of 4-NP showed an increasing trend with temperatures from 298 K to 333 K and in the pH range from 5 to 10 SI: Fig. S4, (SI: Table.T1).

The value of k_{app} is, however, dependent on the amount of catalyst (SI: Table. 1) and hence true catalytic activity of the catalyst cannot be apparently inferred from the k_{app} values. Hence, we calculated the turn over frequency (TOF), the number of moles of 4-NP reduced per mole of Ag per unit time of the catalysts. The TOF values of the Ag(E)-SiO_2 and Ag(seed)-SiO_2(p-TSA^-) are 13.2 s^{-1} and 3.1 s^{-1}, respectively. Table 2 reveals that Ag(E)-SiO_2 catalyst exhibited much higher TOF in comparison with various metal-SiO_2 supported catalysts reported

in literature.[67-70] The above results showed that Ag(E)-SiO_2 possessed superior high catalytic activity and justified our new approach for loading of Ag NPs on to SiO_2 surface. In addition, it is worth mentioning that the Ag(E)-SiO_2 synthesis is simple than previously reported Ag-SiO_2 supported catalysts with a lower loading of Ag NPs.

3.3.1.1. Reusability and stability of Ag(E)-SiO_2 catalyst

We investigated the reusability and stability of Ag(E)-SiO_2 because they are important parameters for a heterogeneous catalyst. The Ag(E)-SiO_2 was recovered from the reaction mixture after the reduction process and re-used subsequently for the reduction of 4-NP. Thus, the recovery-reuse cycling experiments were performed for 5 cycles. The recycling experiments were carried out under the conditions; [4-NP] = 0.5 mM, catalyst amount = 0.25g/L and [$NaBH_4$] = 50 mM. Under the above experimental conditions, the CE% was 100% by 10 min for the 4-NP reduction in the first cycle. We estimated the reusability through two ways. Firstly, the recyclability was assessed by utilizing the catalyst successively for multiple 4-NP reduction cycles and determining the CE% at 10 min for every successive cycles. The catalyst was recovered (experimental section) from the solution after the completion of reduction (CE = 100%) in the first cycle and used for the subsequent cycle successively. The CE% for the subsequent cycle was noticed at 10 min (Fig. 8). The CE% was nearly the same in first two cycles and decreased marginally (CE ~97%) even after 5 cycles. Hence, the Ag(E)-SiO_2 catalyst did not significantly loss catalytic activity up to 5 cycles. Secondly, we have assessed checked the reusability of Ag(E)-SiO_2 catalyst through a comparison of time required for achieving 100% CE in repeated cycles. The required time increased only by 2 min upto 5 cycles which implied a slight decrease in catalytic efficiency after 5 cycles. The extension of the reaction time could be possibly due to two reasons. Firstly, there could be a small loss of Ag NPs from the SiO_2 support.

Secondly, there could be a decrease in the surface activity by morphological modifications or masking of the catalytic sites by the formed product. These two issues are therefore related to the stability of the Ag(E)-SiO_2 catalyst. We tested the stability of the Ag(E)-SiO_2 catalyst by leaching experiments. After the cycle experiment, the catalyst was filtered and the supertenant liquid was separated. The catalytic activity of the supertenant liquid was tested towards 4-NP reduction. The supertenant liquid did not show any catalytic activity over a long time (>4 h) as the absorbance at 400 nm remained nearly invariant over time. This suggested that there could not be any loss of Ag NP from the catalyst surface during the reduction process up to 5 cycles. FESEM observation of the recovered catalyst after 5 cycles revealed that the catalyst retained its morphology and the Ag elemental composition. The experiments on recyclability and stability of Ag(E)-SiO_2 catalyst revealed two concurrent observations. First, there was negligible weight loss of catalyst during cycling process (up to ~5 cycles). Second, Ag NPs were not leached from the catalyst surface. These observations clearly demonstrated the excellent stability and recyclability of the Ag(E)-SiO_2 catalyst. The strong binding interactions between Ag NPs and the amine/imine sites at the SiO_2 surface conform excellent stability and recyclability to Ag(E)-SiO_2 catalyst. The marginal decrease (~2 to 3%) in catalytic activity after two cycles could be ascribed to the probable adsorption of intermediate species/product at the catalytic sites.

3.3.2 Reduction of MB by Ag(E)-SiO_2 catalyst

Our results clearly demonstrated that Ag(E)-SiO_2 catalyst exhibited high catalytic activities toward reduction of 4-NP. Inspired by catalytic the performances of Ag(E)-SiO_2 towards 4-NP reduction, we investigated the catalytic performance of Ag(E)-SiO_2 for an another water pollutant, MB. MB can be reduced to leucomethylene blue at ambient condition in the presence of $NaBH_4$, however, through a very slow reduction rate. The reaction rate of MB can be

accelerated in the presence of catalytic particles. Preliminary observation through naked eye clearly revealed that the blue colour of MB diminished in the presence of Ag(E)-SiO_2. The reduction of MB (0.5mM) was therefore monitored by UV-visible spectroscopy through the changes in absorbances at 664 nm in the presence of 50 mM $NaBH_4$ and 0.25 g/L Ag(E)-SiO_2 catalyst or Ag(seed)-SiO_2(p-TSA^-) catalyst. Fig. 9(A-B) shows the corresponding UV-visible spectra of the mixture recorded over a period. The absorption peak at 664 nm completely vanished at 5 min for Ag(E)-SiO_2 and at 9 min for Ag(seed)-SiO_2(p-TSA^-) and the solution changed from blue to colourless in that process. Alternatively, after 5 min of reaction, the CE% was 100% for Ag(E)-SiO_2 catalyst and 68% for Ag(seed)-SiO_2(p-TSA^-) catalyst. Based on the above results it could be concluded that Ag(E)-SiO_2 has excellent catalytic performance for the reduction of MB. The $\ln(c_o/c_t)$ *versus (vs)* time plots in Fig. 9 (inset) were linear (R^2=0.998 and 0.997, respectively for A and B) and agreed with the pseudo first order reaction kinetics for MB reduction. The rate constant of MB reduction [k_{app}^{MB}] was calculated as 13.4×10^{-2} s^{-1} and 4.03×10^{-3} s^{-1} for Ag(E)-SiO_2 and Ag(seed)-SiO_2(p-TSA^-), respectively. The TOF values were estimated to be 16.7 s^{-1} and 5.04 s^{-1} for Ag(E)-SiO_2 and Ag(seed)-SiO_2(p-TSA^-), respectively. Notably, the catalyst exhibited significantly higher catalytic performance than reported catalysts (Table. 3).[71-73]

3.4 Catalytic mechanism

A probable mechanism of catalysis by Ag(E)-SiO_2 is briefly presented. The rate of reduction for 4-NP or MB increased with the amount of Ag NPs on SiO_2 and the reduction reaction was absent in the absence of Ag NPs. These observations indicated that Ag NPs play the role of a catalyst for the reduction of 4-NP or MB. The catalytic process can be explained by an electrochemical mechanism or chemisorption processes. In the electrochemical mechanism, Ag(E)-SiO_2 serves as

an electron relay for an oxidant and a reductant, and the electron transfer process occurs via the supported Ag NPs. It is presented, that 4-NP or MB may be electrophilic and BH_4^- ions are neoelectrophilic with regards to Ag NPs. Hence, BH_4^- ions can donate electrons to Ag NPs and 4-NP or MB can capture electron from the Ag NPs. In the chemisorption process, both BH_4^- ions and 4-NB or MB may be co-adsorbed on the surface of Ag NPs and electron transfer from MB or 4-NB is probable (J. Phys. Chem. 103, 115 (1999)). The enchanted catalytic activity for Ag(E)-SiO_2 is due to the larger number of active sites (Ag NPs) available on SiO_2 surface.

4. Conclusions

In summary, we have demonstrated a simple "seed mediated strategy" to prepare SiO_2 supported catalyst with enriched Ag NPs (upto 80% weight %) on SiO_2 surfaces. Nearly uniform sized SiO_2 particles (~600 nm) and narrow size distributed (6 to 7 nm) Ag NPs were simultaneously obtained at the seed stage along with functionalized groups (p-TSA^- ions). The electrostatic interactions between p-TSA^- and Ag^+ ions were subsequently utilized towards excessive loading of Ag NPs. Importantly, larger number of Ag NPs with sizes (6-7 nm) similar to the size of Ag NPs in the seed stage were anchored onto the surface of SiO_2 support. The as prepared (Ag(E)-SiO_2) showed excellent catalytic efficiencies towards reduction of 4-nitrophenol and methylene blue and the reduction rate constants ($10.56x10^{-3}$ s^{-1} for 4-NP and $13.4x10^{-2}$ s^{-1} for MB) were comparatively higher than reported in literature for the other Ag based supported catalysts (Table 1 and 2). Our new seed mediated approach to synthesize Ag(E)-SiO_2 catalyst is attractive for the following reasons: i) A higher loading capacity (80% weight %) of Ag NPs was achieved with similar (~7 nm) uniform sizes; ii) the Ag(E)-SiO_2 catalyst exhibited superior catalytic performances for the degradation of organic pollutants (4-NP and MB) (Table 1 and 2) and iii) the methodology provides scope for extended synthesis of various silica@metal catalysts using

other metal ions and adequate functionalization at the silica core. Thus, the present strategy presented a new paradigm for the preparation of several silica@metal support catalysts with denses metallic nanoshells, which in turn could be utilized for varieties of other catalytic reactions and applications.

Acknowledgements

This work was supported by the Priority Research Center Program through a National Research Foundation of Korea (NRF) grant funded by the Ministry of Education, Science and Technology (2009–0093819) and National Research Foundation of Korea (2014-R1A1A4A03004026)

References

1 K. H. Lim, A. B. Mohammad, I. V. Yudanov, K. M. Neyman, M. Bron, P. Claus and N. Rosch, *J. Phys. Chem. C.,* 2009, **113**, 13231-13240.

2 G. Vile, D. Baudouin, I. N. Remediakis, C. Copret, N. Lpez, and J. P. Ramrez, *ChemCatChem,* 2013, **5**, 3750-3759.

3 W. Long, N. A. Brunelli, S. A. Didas, E. W. Ping, and C. W. Jones, *ACS Catal.,* 2013, **3**, 1700–1708.

4 K. M. Manesh, A. I. Gopalan, K. P. Lee and S. Komathi, *Catal. Commun.,* 2010, **11**, 913-918.

5 V. Ambrogi, A. Donnadio, D. Pietrella, L. Latterini, F. A. Proietti, F. Marmottini, G. Padeletti, S. Kaciulis, S. Giovagnoli and M. Ricci, *J. Mater. Chem. B*, 2014, **2**, 6054-6063.

6 L. Han, H. Wei, B. Tu and D. Zhao, *Chem. Commun.*, 2011, 47, 8536-8538.

7 J. M. Li, W. F. Ma, C. Wei, J. Guo, J. Hu and C. C. Wang, *J. Mater. Chem.*, 2011, **21**, 5992-5998.

8 Y. Tian, J. Qi, W. Zhang, Q. Cai, and X. Jiang, *ACS Appl. Mater. Interfaces*, 2014, **6**, 12038−12045.

9 Z. Jiang, J. Zhu, D. Liu, W. Wei, J. Xie and M. Chena, *CrystEngComm*, 2014,**16**, 2384-2394.

10 R. K. Narayanan and S. J. Devaki, *Ind. Eng. Chem. Res.*, 2015, **54**, 1197–1203.

11 Y. Wang, K. Wang, B. Zou, T. Gao, X. Zhang, Z. Du and S. Zhou, *J. Mater. Chem. C*, 2013, **1**, 2441-2447.

12 K. H. Chen, Y. C. Pu, K. D. Chang, Y. F. Liang, C. M. Liu, J. W. Yeh, H. C. Shih, and Y. J. Hsu, *J. Phys. Chem. C.,* 2012, **116**, 19039−19045.

13 L. Rainville, M. C. Dorais and D. Boudreau, *RSC Adv.*, 2013, **3**, 13953-13960.

14 R. J. White, R. Luque, V. L. Budarin, J. H. Clark and D. J. Macquarrie, *Chem. Soc. Rev.*, 2009, **38**, 481-494.

15 X. W. Lou, L. A. Archer and Z. Yang, *Adv. Mater.*, 2008, **20**, 3987–4019.

16 A. Mignani, S. Fazzini, B. Ballarin, E. Boanini, M. C. Cassani, C. Maccato, D. Barreca and D. Nanni, *RSC Adv.*, 2015, **5**, 9600-9606.

17 K. R. Brown, D. G. Walter, and M. J. Natan, *Chem. Mater.*, 2000, **12**, 306–313.

18 W. Niu, L. Zhang and G. Xu, *Nanoscale*, 2013, **5**, 3172-3181.

19 J. H. Kim, W. W. Bryan , H. W. Chung , C. Y. Park , A. J. Jacobson and T. R. Lee, *ACS Appl. Mater. Interfaces*, 2009, **1**, 1063–1069.

20 T. Liu, D. Li, D. Yanga and M. Jiang, *Chem. Commun.*, 2011, **47**, 5169–5171.

21 J. Zhang, J. Liu, S. Wang, P. Zhan, Z. Wang and N. Ming, *Adv. Funct. Mater*, 2004, **14**, 1089-1096.

22 H. G. Lee, G. Sai-Anand, S. Komathi, A. I. Gopalana, S. W. Kang and K. P. Lee, *J. Hazard. Mater*, 2015, **283**, 400–409.

23 Y. Kobayashi, V. S. Maceira, and L. M. Liz-Marzan, *Chem. Mater.*, 2001, **13**, 1630–1633.

24 C. L. Kielkopf, S. White, J. W. Szewczyk, J. M. Turner, E. E. Baird, P. B. Dervan and D. C. Rees, *Science*, 1998, **282**, 111-115.

25 T. Cassagneau and F. Caruso, *Adv. Mater.,* 2002, **14**, 732-736.

26 K. P. Lee, A. M. Showkat, A. I. Gopalan, S. H. Kim, and S. H. Choi, *Macromolecules*, 2005, **38**, 364-371.

27 K. M. Manesh, A. I. Gopalan, K. P. Lee, N. H. Kim, S. Komathi and S. H. Kang, *J. Polym. Sci. A Polym. Chem.,* 2010, **48**, 4537–4546.

28 P. Santhosh, K. M. Manesh, S. Uthayakumar, A. I. Gopalan and K. P. Lee, *Biosens. Bioelectron.*, 2009, **24**, 2008-2014.

29 K. M. Manesh, P. Santhosh, S. Uthayakumar, A. I. Gopalan and K. P. Lee, *Biosens. Bioelectron.*, 2010, **25**, 1579–1586.

30 G. Sai Anand, A. I. Gopalan, S. W. Kang and K. P. Lee, *J. Anal. At. Spectrom.*, 2013, **28**, 488-498.

31 S. K. Park, K. D. Kim and H. T. Kim, *Colloids and Surfaces A: Physicochem. Eng. Aspects* 2002, **197**, 7–17.

32 M. P. Pileni, *Nat. Mater.*, 2003, **2**, 145 – 150.

33 H. G Woo and T. D. Tilley, *J. Am. Chem. Soc.*, 1989, **111**, 8043.

34 Ji. Guo, X. Liu, Y. Cheng, Y. Li, G. Xu and P. Cui, *J. Colloid. Interface. Sci.*, 2008, **326**, 138–142.

35 W. Stober and A. Fink, *J. Colloid Interface Sci.*, 1968, **26**, 62-69.

36 K. S. Finnie, J. R. Bartlett, C. J. Barbe and L. Kong, *Langmuir.* 2007, **23**, 3017-3024.

37 K. D. Hartlen, A. P. T. Athanasopoulos, and V. Kitaev, *Langmuir*, 2008, **24**, 1714–1720.

38 K. Sato, T. Yoshinari, Y. Kintaichi, M. Haneda and H. Hamada, *Appl. Catal. B.*, 2003, **44**, 67–78.

39 C. Shi, M. Cheng, Z. Qu And Xinhe Bao, *J. Mol. Catal. A: Chem.,* 2005, **235**, 35–43.

40 S. Arunsawad, K. Srikulkit and S. Limpanart, *J. Met. Mater. Miner.,* 2010, **20**, 29–34.

41 L. Jiang, Z. Wu, D. Wu, W. Yang and R. Jin, *Nanotech.*, 2007, **18**, 185603/1-185603/6.

42 G. Sai-Anand, A. I. Gopalan, S. W. Kang, S. Komathi and K. P. Lee, *Sci. Adv. Mater.*, 2014, **6**, 1356-1364.

43 P. Zhang, L. Wang, J. Xie, L. Su and C. Ma, *J. Mater. Chem. A*, 2014, **2**, 3776-3782.

44 Y. Gao, D. Shan, F. Cao, J. Gong, X. Li, H. Ma, Z. Su and L. Qu, *J. Mater. Chem. C*, 2009, **113**, 15175–15181.

45 Y. C. Liu and T. C. Chuang, *J. Phys. Chem. B*, 2003, **107**, 12383–12386.

46 C. Mangeney, S. Bousalem, C. Connan, M. J. Vaulay, S. Bernard, and M. M. Chehimi, *Langmuir*, 2003, **19**, 5511-5516.

47 S. N. Kumar, F. Gaillard, G. Bouyssoux and A. Sartre, *Synt. Met.*, 1990, **36**, 111 – 127.

48 M. Trchova, I. Sedenkova, E. N. Konyushenko, J. Stejskal, P. Holler, and G. C. Marjanovic, *J. Phys. Chem. B*, 2006, **110**, 9461–9468.

49 E. C. Venancio, P. C. Wang, and A. G. MacDiarmid, *Synt. Met.*, 2006, **156**, 357–369.

50 M. Trchova, I. Sedenkova, E. N. Konyushenko, J. Stejskal, P. Holler, and G. Ciric-Marjanovic, *J. Phys. Chem. B*, 2006, **110**, 9461–9468.

51 Z. Dong, X. Le, C. Dong, W. Zhang, X. Li, and J. Ma, *Appl. Catal. B-Environ*, 2015, **162**, 372-380.

52 M. Ghaedi, Sh. Heidarpour, S. N. Kokhdan, R. Sahraie, A. Daneshfar, and B. Brazesh *Powder Technol*, 2012, **228**, 18–25.

53 C. Wang, F. Yang, W. Yang, L. Ren, Y. Zhang, X. Jia, L. Zhang and Y. Li, *RSC Adv.*, 2015, **5**, 27526-27532.

54 Y. Lu, Y. Mei1, M. Drechsler and M. Ballauff, *Angew. Chem. Int. Ed.*, 2006, **45**, 813 –816.

55 Y. Mei, G. Sharma, Y. Lu, and M. Ballauff, *Langmuir*, 2005, **21**, 12229–12234.

56 J. Min, F. Wang, Y. Cai, S. Liang, Z. Zhang and X. Jiang, *Chem. Commun.*, 2015, **51**, 761-764.

57 W. Wu, M. Lei, S. Yang, L. Zhou, L. Liu, X. Xiao, C. Jiang and V. A. L. Roy, *J. Mater. Chem. A*, 2015, **3**, 3450-3455.

58 Y. Lu, P. Spyra, Y. Mei, M. Ballauff, and A. Pich, *Macromol. Chem. Phys.*, 2007, **208**, 254–261.

59 N. Pradhan, A. Pal and T. Pal, *Colloid Surface A*, 2002, **196**, 247–257.

60 S. V. Otari, R. M. Patil, S. R. Waghmare, S. J. Ghosh and S. H. Pawar, *Dalton Trans.*, 2013, **42**, 9966-9975.

61 L. Ai, H. Yue and J. Jiang, *J. Mater. Chem.*, 2012, **22**, 23447-23453.

62 S. Tang, S. Vongehr and X. Meng, *J. Phys. Chem. C*, 2010, **114**, 977–982.

63 S. Wang, J. Zhang, P. Yuan, Q. Sun, Y. Jia, W, Yan, Z, Chen, and Q. Xu, *J. Mater. Sci*, 2015, **50**, 1323-1332.

64 Md. H. Rashid and T. K. Mandal, *J. Phys. Chem. C*, 2007, **111**, 16750–16760.

65 Y. Chi, Q. Yuan, Y. Li, J. Tu, L. Zhao, N. Li and X. Li, *J Colloid Interface Sci.*, 2012, **383**, 96-102.

66 M. Wang, D. Tian, P. Tian, and L. Yuan, *Appl. Surf. Sci.*, 2013, **283**, 389– 395.

67 Z. Wang, H. Fu, D. Han and F. Gu, *J. Mater. Chem. A*, 2014, **2**, 20374-20381.

68 Y. Deng , Y. Cai, Z. Sun , J. Liu , C. Liu , J. Wei , W. Li , C. Liu , Y. Wang and D. Zhao, *J. Am. Chem. Soc.*, 2010, **132**, 8466–8473.

69 W. Wang, Z. Meng, Q. Zhang, X. Jia and K. Xi. *J Colloid Interface Sci.*, 2014, **418**, 1-7.

70 W. Li, A. Wang, X. Yang, Y. Huang and T. Zhang, *Chem. Commun.*, 2012, **48**, 9183–9185.

71 M. M. Khan, J. Lee and M. H. Cho, *J. Ind. Eng. Chem.*, 2014, **20**, 1584-1590.

72 Y. Tang, T. Wu, B. Hu, Q. Yang, L. Liu, B. Yu, Y. Ding and S. Ye, *Mater. Chem. Phys.*, 2015, **149-150**, 460-466.

73 V.S. Suvith and D. Philip, *Spectrochim Acta A*, 2014, **118**, 526-532.

74 N. R. Jana, T. K. Sau, and T. Pal, *J. Phys. Chem. B*., 1999, **103**, 115–121.

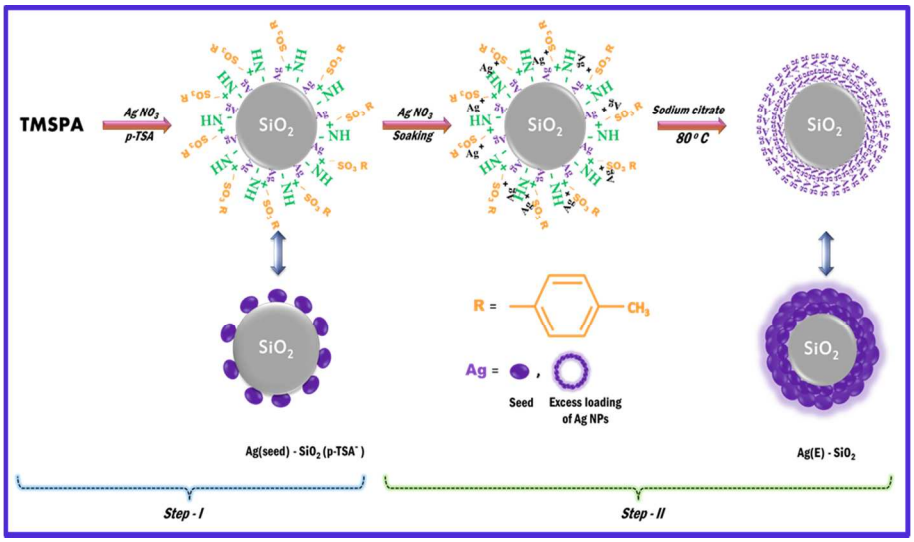

Scheme 1 New "seed-mediated" strategy toward higher loading of Ag NPs onto SiO_2 support. *Step-I*: Preparation of "seed" Ag NPs embedded functionalized SiO_2 sphere (Ag(seed)-SiO_2(p-TSA^-)) by simultaneous formation of p-TSA^- functionalized SiO_2 sphere and Ag NPs (seed). *Step-II*: Preparation of Ag(E)-SiO_2 via extended deposition of Ag NPs onto SiO_2 sphere. The surface of Ag(seed)-SiO_2(p-TSA^-) contains negative (p-TSA^- ion) charges for effective accumulation of Ag^+ ions onto the surface. The higher loading of Ag NPs was achieved by reduction with sodium citrate (p-TSA^- = p-toluene sulfonic acid).

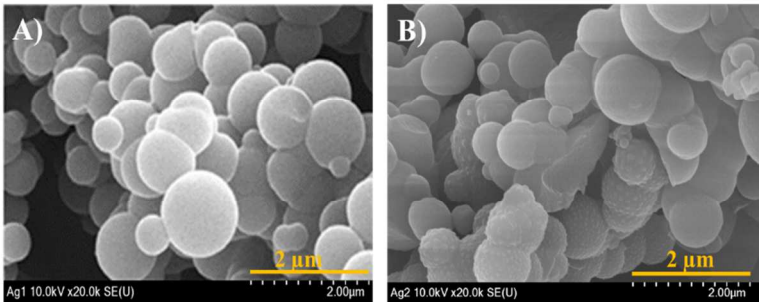

Fig. 1 FESEM image of **A)** Pristine SiO_2 (PTMSPA) and **B)** Ag(seed)-SiO_2(p-TSA^-).

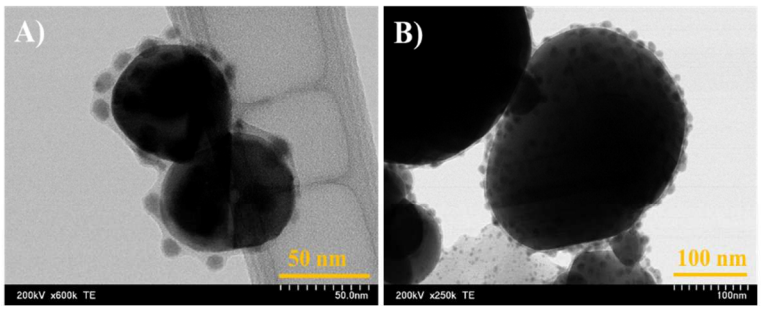

Fig. 2 TEM images of **A)** Ag(seed)-SiO_2(p-TSA^-) and **B)** Ag(E)-SiO_2.

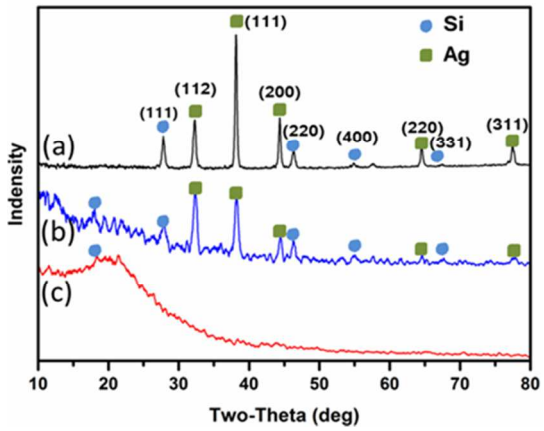

Fig. 3 XRD patterns of **(a)** Ag(E)-SiO_2, **(b)** Ag(seed)-SiO_2(p-TSA^-) and **(c)** pristine SiO_2.

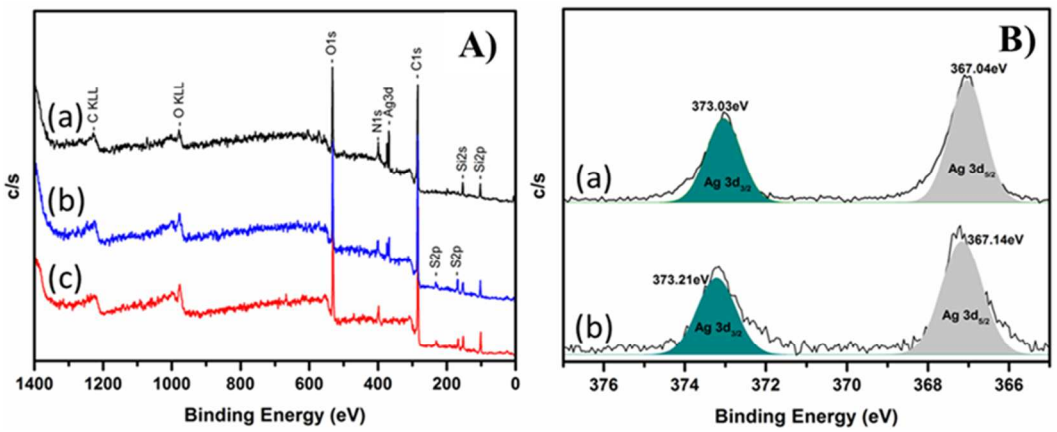

Fig. 4 (**A)** Survey level XPS spectrum of **(a)** Ag(E)-SiO_2, **(b)** Ag(seed)-SiO_2(p-TSA^-) and **(c)** pristine SiO_2 and **B)** XPS Ag core level spectrum of **(a)** Ag(E)-SiO_2 and **(b)**Ag(seed)-SiO_2(p-TSA^-).

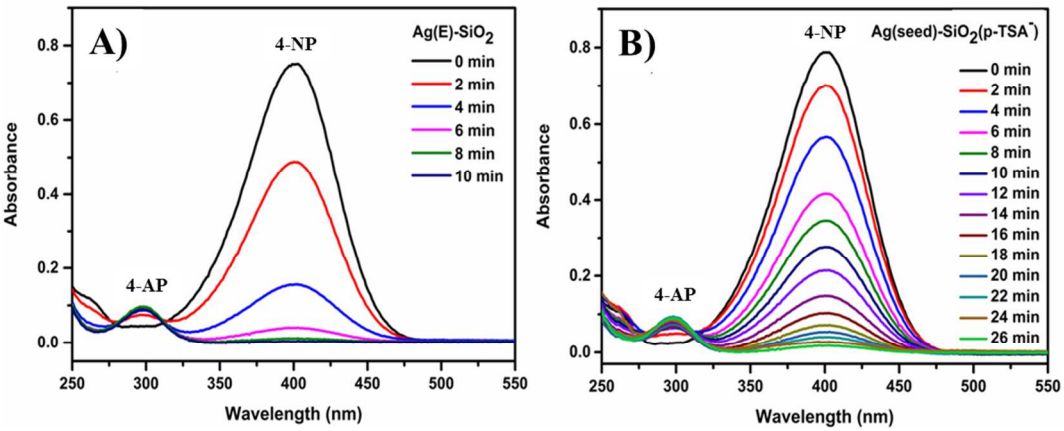

Fig. 5 Successive UV–vis spectra recorded during the reduction of 4-NP in the presence of **A)** Ag(E)-SiO_2 and **B)** Ag(seed)-SiO_2(p-TSA^-) catalysts; Amount of catalyst =0.25 g/L, [$NaBH_4$] = 50 mM and [4-NP]= 0.5 mM.

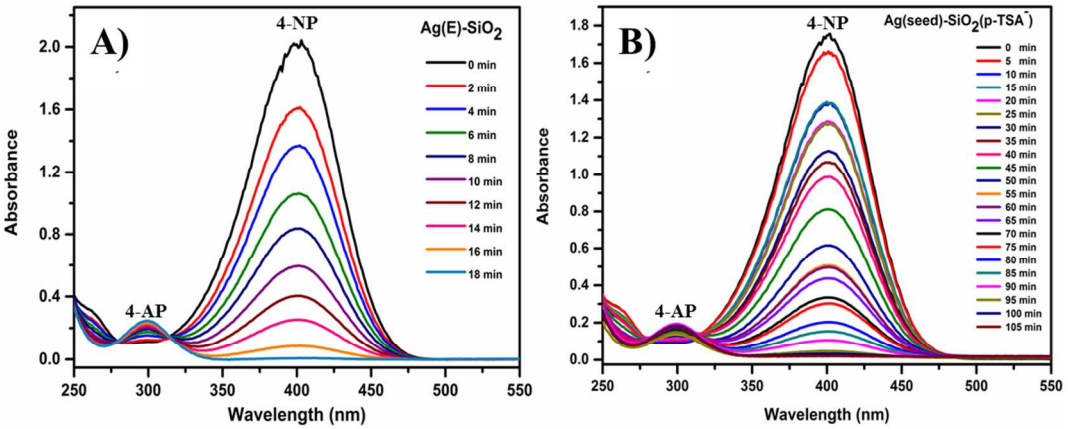

Fig. 6 Successive UV–vis spectra recorded during the reduction of 4-NP in presence of **A)** Ag(E)-SiO_2 and **B)** Ag(seed)-SiO_2(p-TSA^-) catalysts; Amount of catalysts =0.25 g/L, [$NaBH_4$] = 50 mM and [4-NP]= 1 mM.

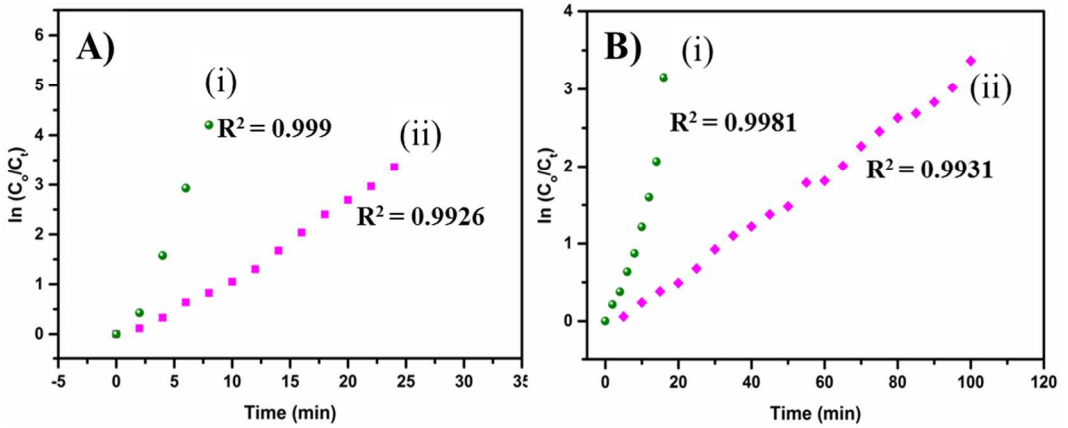

Fig. 7 (A, B) Plots of ln (c_o/c_t) virsus time for **i)** Ag(E)-SiO_2 and **ii)** Ag(seed)-SiO_2(p-TSA^-) catalyst; Amount of catalyst =0.25 g/L(**A,B**), [$NaBH_4$] = 50 mM(**A,B**), [4-NP]= 0.5 mM **(A) and** 1.0 mM **(B)**

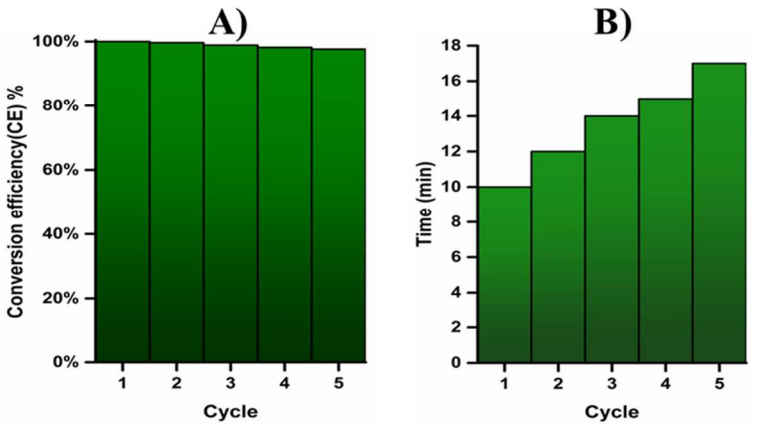

Fig. 8 (A) Recycling performance for the catalytic activity toward 4-NP reduction with Ag(E)-SiO_2 catalyst. The time for 2-5 cycles was set as the time required for achieving 100% in the first cycle. **B)** The time required for achieving 100% catalytic conversion efficiency for repeated cycle was determined.

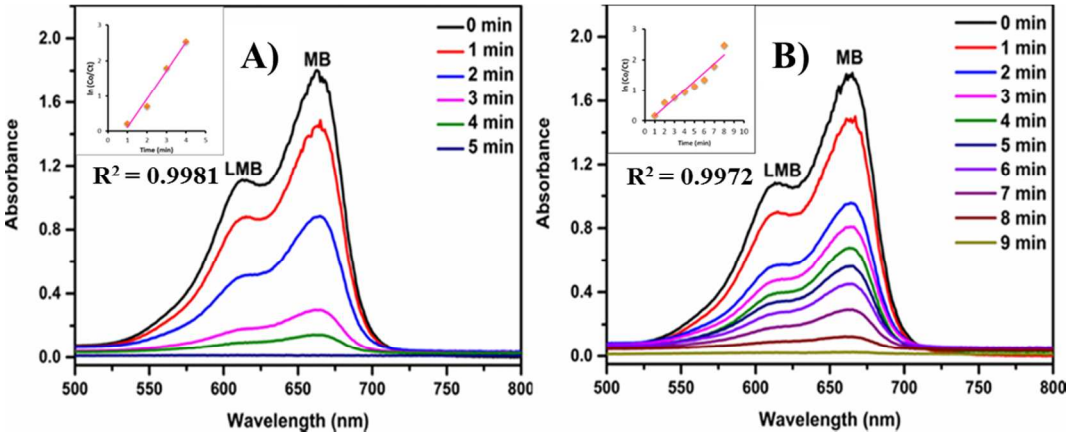

Fig. 9 Successive UV–vis spectra recorded during the reduction of MB in presence of **A)** Ag(E)-SiO_2 and **B)** Ag(seed)-SiO_2(p-TSA^-) catalysts; amount of catalysts =0.25 g/L, [$NaBH_4$] = 50 mM, [MB]= 0.5 mM; Inset corresponds to plot of ln (c_o/c_t) vs. time for reduction of MB

Table 1 Comparison of rate constant for 4-nitrophenol reduction by Ag nanoparticles and Ag supported catalysts.

Catalyst	*Rate constant(k) x 10^{-3} (s^{-1})	Reference
Ag NPs	3.83	56
Ag NPs ($Cu_{precursor}$= 0mg)	0.47	57
Cu/Ag NPs ($Cu_{precursor}$= 9mg)	2.10	57
Cu/Ag NPs ($Cu_{precursor}$= 18mg)	3.94	57
Cu/Ag NPs ($Cu_{precursor}$= 27mg)	3.46	57
PVA/PS-PEG MA/Ag	0.078	58
PVA/Ag	0.0004	59
Ag/Alg biohydrogel	6.00	60
Alginate-magnetic hybrid/Ag hydrogel	4.50	61
Ag/C spheres	1.69	62
Ag NPs-SCT	8.00	56
Ag@RMF NSs	< 10	63
triammonium citrate (TAC)-Ag-1.0	5.19	64
Fe_3O_4-@SiO_2-Ag	7.67	65
Micron-SiO_2@nano-Ag	3.56	66
Ag@SiO_2 NSs	< 5	63
Ag(seed)-SiO_2(p-TSA^-)	2.48	This work
Ag (E)-SiO_2	10.56	This work

(*depends on catalyst amount)

Table 2 Comparison of turn over frequency (TOF) for 4-nitrophenol reduction by metal/SiO_2 supported catalysts.

Catalyst	TOF (min^{-1})	Reference
Au@SiO_2	0.45	67
Fe_3O_4@SiO_2-Au@m SiO_2	0.30	68
Monodispers Au-SiO_2	17.7	69
Au/SiO_2 (H_2O)	16.5	70
Au/SiO_2 (Ethyl acetate)	11.0	70
Ag(seed)-SiO_2(p-TSA^-)	186	This work
Ag (E)-SiO_2	792	This work

Table 3 Comparison of rate constant for the degradation of MB by Ag NP supported onto various materials.

Catalyst	*Rate constant(k) x 10^{-3} (s^{-1})	Reference
Au@TiO_2	2.60	71
TiO_2	1.26	71
Ag NPs/P(NIPAM-co-DMA)-1	0.97	72
Ag NPs/P(NIPAM-co-DMA)-2	0.83	72
Ag NPs/P(NIPAM-co-DMA)-3	0.90	72
(Ag NPs (s) and Au NPs(g) colloids) s_5	2.50	73
(Ag NPs (s) and Au NPs(g) colloids) s_8	3.73	73
(Ag NPs (s) and Au NPs(g) colloids) g_1	2.20	73
(Ag NPs (s) and Au NPs(g) colloids) g_5	5.51	73
(Ag NPs (s) and Au NPs(g) colloids) g_8	11.13	73
Ag(seed)-SiO_2(p-TSA^-)	4.03	This work
Ag (E)-SiO_2	13.4	This work

(*depends on catalyst amount)

Graphical Abstract

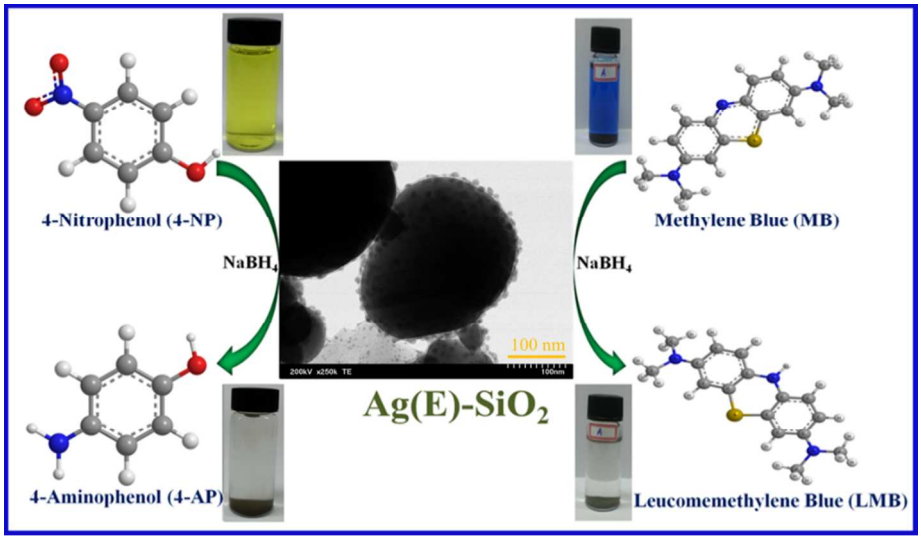

The facile route to higher loading of silver nanoparticles onto silica support is useful for large-scale synthesis of efficient silver supported catalysts.